NASA Technical Memorandum 106173
AIAA–93–1927
CMOTT–93–9

A Critical Comparison of Several Low Reynolds Number k-ε Turbulence Models for Flow Over a Backward-Facing Step

C.J. Steffen, Jr.
Center for Modeling of Turbulence and Transition
Lewis Research Center
Cleveland, Ohio

Prepared for the
29th AIAA Joint Propulsion Conference and Exhibit
cosponsored by the AIAA, SAE, ASME, and ASEE
Monterey, California, June 28–30, 1993

NASA

A CRITICAL COMPARISON OF SEVERAL LOW REYNOLDS NUMBER k-ϵ TURBULENCE MODELS FOR FLOW OVER A BACKWARD-FACING STEP

Christopher J. Steffen, Jr.*
Center for Modeling of Turbulence and Transition (CMOTT)
NASA Lewis Research Center, Cleveland, Ohio

Abstract

Turbulent backward-facing step flow was examined using four low turbulent Reynolds number k-ϵ models and one standard high Reynolds number technique. A tunnel configuration of 1:9 (step height: exit tunnel height) was used. The models tested include: the original Jones and Launder; Chien; Launder and Sharma; and the recent Shih and Lumley formulation. The experimental reference of Driver and Seegmiller was used to make detailed comparisons between reattachment length, velocity, pressure, turbulent kinetic energy, Reynolds shear stress, and skin friction predictions. The results indicated that the use of a wall function for the standard k-ϵ technique did not reduce the calculation accuracy for this separated flow when compared to the low turbulent Reynolds number techniques.

Introduction

For the past two decades, researchers interested in evaluating wall bounded flows have relied upon two equation turbulence models to facilitate this effort. In the context of the Reynolds Averaged Navier Stokes (RANS) equations, this involved an assumption that the closure problem has been bridged by the Boussinesq approximation. This approximation relates the Reynolds stress tensor to the velocity gradient tensor via an eddy viscosity. The family of two equation models defined this eddy viscosity in terms of characteristic turbulent velocity and length scales which resulted from the solution of two additional partial differential equations. One example of this theory is the energy-dissipation rate (k-ϵ) model. However, for wall bounded flows, the two turbulent transport equations behave differently for each separate region of near-wall flow. Modelling this near-wall flow behavior is crucial to the success of an internal flow simulation.

One of the more challenging internal flows used to benchmark a given model is the backward-facing step (BFS). The presence of a strong recirculation bubble, a reattaching shear layer, a redeveloping channel flow and a relatively simple geometry have made this a particularly attractive flow to analyze; it has become a de facto "complex canonical" flow[1]. BFS flow is an excellent candidate for examining the relationship of near-wall treatment to the k-ϵ model performance for separated flows.

Two definite schools of thought have emerged on how to treat this region of low turbulent Reynolds number (Re_t) flow near a solid surface. The standard, or high Re_t (HR) formulations utilized wall functions to model the near-wall flow, while the low Re_t (LR) formulations incorporated the use of damping functions to model the effects of this region.

At a first glance, the empiricism involved in the use of wall functions tends to make the more sophisticated LR models appear more attractive. Wall functions were based solely upon the behavior of attached equilibrium turbulent flow. There is, however, a significant cost savings to be realized from the appropriate use of HR models in terms of grid size. Alternatively, the LR models offer the ability to solve the transport equations through the viscous sublayer. Thus a straightforward boundary condition procedure is applied at the wall. This permits the near-wall velocity gradient to be found as a result of the calculation, not merely as an a priori assumption. It is this feature which has attracted such a great deal of attention to these LR models in the past two decades. However, the development of these models was also primarily based upon the characteristics of attached bo ndary layer flow as well.

Although much effort has recently been expended on the study of BFS flow with the k-ϵ model, the overwhelming majority of analysis has utilized the wall function approach due to the reduced numerical complexity. To the author's knowledge, only So et al.[2] and Avva et al.[3] have examined the LR k-ϵ formulation for BFS, and this was limited to the Chien model. While this model is known to be quite robust for a wide variety of flows, an anomalous behavior exists near the separation and reattachment points. This will be discussed in detail later. Several LR k-ϵ models exist which do not demonstrate this same behavior for separated flow.

The intention of this study is to investigate several LR models and compare against the performance of the HR formulation for separating flow. The first section describes the governing equations and turbulence models, as well as the experimental study of backward-facing step flow by Driver and Seegmiller[4]. The following section details the numerical methods used for this simulation. The final two sections include a discussion of the results and the conclusions of this research.

*Aerospace Engineer, Computational Fluid Dynamics Branch; Member AIAA

Background

Governing Equations

The RANS equations for incompressible flow are shown below in equation system 1. The dependent variables include the pressure and velocity as well as the Reynolds stress tensor, $\langle\overline{u_i u_j}\rangle$. Here the quantities (P,U,V) denote the mean values while (p,u,v) are the fluctuating components.

$$\begin{aligned} U_{i,i} &= 0 \\ U_{i,t} + U_j U_{i,j} + \frac{1}{\rho}P_{,i} - \nu U_{i,jj} + \langle\overline{u_i u_j}\rangle_{,j} &= 0 \end{aligned} \tag{1}$$

The Boussinesq approximation closes the system by assuming the relation given in equations 2.

$$\begin{aligned} \overline{u_i u_j} &= -\nu_t(U_{i,j} + U_{j,i}) + \frac{2}{3}k\delta_{ij} \\ k &= \frac{1}{2}\overline{u_i u_i} \end{aligned} \tag{2}$$

Notice that this is a function of the mean velocity gradients and the turbulent kinetic energy, k. Now the eddy viscosity must be modelled. Gas kinetic theory yields a definition of the kinematic viscosity as a function of characteristic velocity and length scales. An eddy viscosity can be formulated if characteristic turbulent velocity and length scales can be postulated. For the k-ϵ models, the velocity scale is given as the square root of k, while the length scale is a ratio involving k and the dissipation rate of turbulent kinetic energy, ϵ. Thus, the isotropic turbulent viscosity is defined as $\nu_t = C_\mu f_\mu \left(\frac{k^2}{\epsilon}\right)$.

Transport equations are used to resolve the values of k and ϵ and are shown here in equation 3.

$$\begin{aligned} k_{,t} + U_j k_{,j} - \left[\left(\nu + \frac{\nu_t}{\sigma_k}\right)k_{,j}\right]_{,j} &= \mathcal{P} - \epsilon + D \\ \epsilon_{,t} + U_j \epsilon_{,j} - \left[\left(\nu + \frac{\nu_t}{\sigma_\epsilon}\right)\epsilon_{,j}\right]_{,j} &= C_1 f_1 \frac{\epsilon}{k}\mathcal{P} - C_2 f_2 \frac{\epsilon^2}{k} + E \end{aligned} \tag{3}$$

where production of turbulent kinetic energy is defined as $\mathcal{P} = -\langle\overline{u_i u_j}\rangle\frac{1}{2}(U_{i,j} + U_{j,i})$. The constants C_μ, C_1, C_2, σ_k and σ_ϵ are defined a priori. The terms D, E, f_μ, f_1 and f_2 are correction terms for the LR formulation and are necessary to give asymptotically correct behavior if the numerical domain is extended to the wall.

k-ϵ Model: HR Formulation

In order to bridge the viscous sublayer, a two layer "law of the wall" was used to establish the values of k_{bc} and ϵ_{bc} at the first point off the wall. The two layer model used in this test is similar to that given in reference[5]. For two dimensional boundary layer flow, the wall function is expressed below.

$$\begin{aligned} u^+ &= \left\{ \begin{array}{ll} y^+ & \text{for } y^+ \le 11 \\ 5.5 + 2.5ln(y^+) & \text{for } y^+ > 11 \end{array} \right\} \\ \text{where} \quad & \begin{aligned} y^+ &= \frac{y u_\tau}{\nu} \\ u^+ &= \frac{U}{u_\tau} \\ u_\tau &= \sqrt{\left(\frac{\tau}{\rho}\right)_{wall}} \end{aligned} \end{aligned} \tag{4}$$

Distance to the nearest wall was specified as (y) and the shear stress was denoted (τ). If one assumed that this first interior grid point was properly positioned at the edge of the buffer layer, then empirical evidence suggests that the production of k was equal to the dissipation of k:

$$\mathcal{P}_{bc} = \epsilon_{bc} \tag{5}$$

The numerical boundary conditions for k_{bc} and ϵ_{bc} were then derived from this *equilibrium* expression combined with the definition of ν_t and equations 4.

$$\frac{k_{bc}}{u_\tau^2} = C_\mu^{-\frac{1}{2}}, \quad \epsilon_{bc} = 2.5C_\mu^{\frac{3}{4}}\frac{k_{bc}^{\frac{3}{2}}}{y} \tag{6}$$

While this assumption is not valid for separated flow due the fact that the logarithmic overlap region is not present for this flow regime, we shall see later that the predictive capability of the HR formulation is not significantly diminished. To complete the model specification, the values of the constants and functions are listed in the tables below.

k-ϵ Model: LR Formulation

Four different LR turbulence models were investigated in this study including: the original Jones and Launder (JL)[6], Chien (CH)[7], Launder and Sharma (LS)[8] and the recent Shih and Lumley (SL)[9] formulation. These models can be grouped into two broad categories according to the form of the near-wall corrections. The JL and LS models were developed as functions of the dependent variables alone, while the CH and SL models were based upon both the dependent and independent variables. All four models can be implemented in a domain extending to the wall. These are just a few of the many different models available, and the interested reader is referred to references [10,11,12] for a more thorough review.

The influence of the viscous dominated near-wall region was affected through the use of explicit damping functions and additional destruction terms. As mentioned earlier, these models were also developed to match the observed behavior of an attached boundary layer flow. Thus these LR formulations also suffer from an inherently empirical nature. The values of these functions, destruction terms, and additional constants are listed in the tables below. Note that for the SL model, the damping function was derived in terms of $Re_k = \frac{k^{\frac{1}{2}}y}{\nu}$, and the following

constants: $a_1 = -1.5 \times 10^{-4}$, $a_3 = -1.0 \times 10^{-9}$, and $a_5 = -5.0 \times 10^{-10}$. The boundary conditions for the JL, LS, and CH models were specified as

$$\epsilon_{bc} = k_{bc} = 0 \tag{7}$$

while for the SL model the boundary conditions were slightly more complicated.

	C_1	C_2	C_μ	σ_k	σ_ϵ
JL	1.55	2.0	0.09	1.0	1.3
LS	1.44	1.92	0.09	1.0	1.3
CH	1.35	1.8	0.09	1.0	1.3
SL	1.44	1.92	0.09	1.0	1.3
HR	1.44	1.92	0.09	1.0	1.3

Table 1 The k-ϵ model constants

	f_1	f_2	f_μ
JL	1.0	$1-.3e^{-Re_t^2}$	$e^{\left(\frac{-2.5}{(1+Re_t/50)}\right)}$
LS	1.0	$1-.3e^{-Re_t^2}$	$e^{\left(\frac{-3.4}{(1+Re_t/50)^2}\right)}$
CH	1.0	$1-.22e^{-\frac{Re_t^2}{36}}$	$1-e^{-0.0115y^+}$
SL	1.0	$1-.22e^{-\frac{Re_t^2}{36}}$	$\left[1-e^{\left(a_1R_k+a_3R_k^3+a_5R_k^5\right)}\right]^{\frac{1}{2}}$
HR	1.0	1.0	1.0

Table 2 The LR k-ϵ damping functions

	D	E
JL	$-2\nu\left(k^{\frac{1}{2}}_{,i}\right)^2$	$2\nu\nu_t U_{i,jk} U_{i,jk}$
LS	$-2\nu\left(k^{\frac{1}{2}}_{,i}\right)^2$	$2\nu\nu_t U_{i,jk} U_{i,jk}$
CH	$-\frac{2\nu k}{y^2}$	$-\frac{2\nu\epsilon}{y^2}e^{-.5y^+}$
SL	0	$\nu\nu_t U_{i,jk} U_{i,jk}$
HR	0	0

Table 3 The LR k-ϵ additional terms

Shih and Lumley have derived boundary conditions based upon an asymptotic behavior in the very near-wall region. As one approaches the wall from outside the boundary layer, a turbulent limit point is reached beyond which self sustaining turbulence cannot exist. If this point is designated by the subscript α, then Shih and Lumley proposed the relations of equation 8.

$$\epsilon_\alpha = 0.251\frac{u_\tau^4}{\nu} \quad , k_\alpha = 0.25u_\tau^2 \tag{8}$$

For practical purposes, this limit point was assumed to extend to the wall; hence $\epsilon_{bc} = \epsilon_\alpha$, $k_{bc} = k_\alpha$.

A comment on implementation in two dimensional flow is necessary for several models. The implementation of HR and SL involved the use of a value (y) which was based upon the minimum distance to a no–slip boundary in the numerical domain. This appeared to work quite well. For the CH model, the minimum y^+ value was used. This straight forward extension of the CH formulation to two dimensions resulted in a grid dependent solution in the region surrounding reattachment.

BFS Flow: Experimental Configuration

Many different experimental data exist for validation of turbulent flow over a backward-facing step. The Stanford conference of 1980–81 used the Kim et al.[13] data for a 1:3 (step height: exit tunnel height) tunnel to benchmark model performance. The velocity profiles were measured via hot wire anemometry. However, turbulence data was unavailable in the recirculation zone. Recently, Kjelgaard[14] has examined backward-facing step flow using a three component laser velocimeter in a 1:2 tunnel configuration. Mean velocity profiles and turbulent normal and shear stresses were tabulated throughout the flow domain. However the experiment of Driver and Seegmiller[4] has been chosen here because the measurements included skin friction, pressure, turbulent normal and shear stress, and velocity profiles from the step downstream through the recovery region. A two component laser velocimeter was used to obtain the velocity and turbulence data. The tunnel expansion ratio of 1:9 (zero deflection angle) produced a much lower pressure gradient due to freestream sudden expansion than the other aforementioned tunnel geometries.

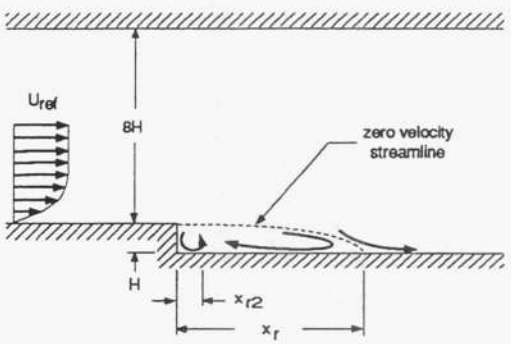

Fig. 1 Tunnel configuration for the backward-facing step of Driver and Seegmiller[4]

The tunnel configuration can be seen here in figure 1. The inlet was 80H upstream from the expansion and the exit was downstream an additional 60H. The experimental Mach number was 0.128. The turbulent boundary

layer thickness was recorded as 1.5H at a location 4 step heights upstream of the expansion. The experiment was conducted at a Reynolds number (Re_H) of 33420, based upon the step height. According to Driver and Seegmiller, this value insured that the boundary layer was fully turbulent as it passed over the step.

Numerical Method

RANS Equations

A modified version of the finite volume code, DTNS2D[15] was chosen for this study. Chorin's[16] pseudo compressibility technique was used to resolve the incompressible RANS equations. The system of equations solved for the two dimensional pseudo compressibility method differs from the incompressible flow equations by the addition of a time dependent term in the continuity equation, $\frac{1}{\beta}\frac{\partial p}{\partial t}$. This is shown in nondimensional form for 2D laminar flow in equations 9. Note that x and y are the independent variables and Re refers to the Reynolds number. The variable (P) is defined as the pressure normalized by the constant density. For turbulent flow, the kinematic viscosity is replaced with the sum of turbulent and kinematic viscosities. This system can be regarded as hyperbolic in nature while the incompressible flow equations are elliptic. The pseudo sound speed, $c = \sqrt{U_c^2 + \beta}$, is governed by the value of the parameter β and the contravariant velocity U_c, whereas the physical sound speed is infinite. For this study, the value of β was set to unity.

$$\frac{\partial}{\partial t}(\mathbf{q}) + \frac{\partial}{\partial x}(\mathbf{f_1}+\mathbf{g_1}) + \frac{\partial}{\partial y}(\mathbf{f_2}+\mathbf{g_2}) = 0$$

$$\mathbf{q} = \begin{bmatrix} \mathrm{P} \\ \mathrm{U} \\ \mathrm{V} \end{bmatrix}, \ \mathbf{f_1} = \begin{bmatrix} \mathrm{U}\beta \\ \mathrm{U}^2+\mathrm{P} \\ \mathrm{UV} \end{bmatrix}, \ \mathbf{f_2} = \begin{bmatrix} \mathrm{V}\beta \\ \mathrm{UV} \\ \mathrm{V}^2+\mathrm{P} \end{bmatrix} \quad (9)$$

$$\mathbf{g_1} = \frac{-1}{Re}\begin{bmatrix} 0 \\ \frac{\partial \mathrm{U}}{\partial x} \\ \frac{\partial \mathrm{V}}{\partial x} \end{bmatrix}, \ \mathbf{g_2} = \frac{-1}{Re}\begin{bmatrix} 0 \\ \frac{\partial \mathrm{U}}{\partial y} \\ \frac{\partial \mathrm{V}}{\partial y} \end{bmatrix}$$

The chief advantage of the pseudo compressibility technique is that the system of equations can now be marched in time towards a steady solution. With this in mind, the approximate factorization scheme was chosen to resolve the governing equations 9. The system is expressed in generalized coordinates $(\xi(x,y), \eta(x,y))$ below in the equation system 10.

$$\frac{\partial}{\partial t}(\hat{\mathbf{q}}) + \frac{\partial}{\partial \xi}\left(\hat{\mathbf{f_1}}+\hat{\mathbf{g_1}}\right) + \frac{\partial}{\partial \eta}\left(\hat{\mathbf{f_2}}+\hat{\mathbf{g_2}}\right) = 0$$

$$\mathrm{J} = \frac{\partial(\xi,\eta)}{\partial(x,y)}, \ \hat{\mathbf{q}} = \frac{\mathbf{q}}{\mathrm{J}}$$

$$\hat{\mathbf{f_1}} = \frac{\xi_x \mathbf{f_1} + \xi_y \mathbf{f_2}}{\mathrm{J}}, \ \hat{\mathbf{f_2}} = \frac{\eta_x \mathbf{f_1} + \eta_y \mathbf{f_2}}{\mathrm{J}} \quad (10)$$

$$\hat{\mathbf{g_1}} = \frac{\xi_x \mathbf{g_1} + \xi_y \mathbf{g_2}}{\mathrm{J}}, \ \hat{\mathbf{g_2}} = \frac{\eta_x \mathbf{g_1} + \eta_y \mathbf{g_2}}{\mathrm{J}}$$

This system can be factored as shown below in equations 11

$$\left\{\frac{\mathbf{V}}{\Delta t} + \frac{\partial^-}{\partial \xi}\mathbf{A}^+ + \frac{\partial^+}{\partial \xi}\mathbf{A}^- + \frac{\partial'}{\partial \xi}\mathbf{A}_v\right\}\Delta\hat{\mathbf{q}}^* = \mathbf{RHS}$$

$$\left\{\frac{\mathbf{V}}{\Delta t} + \frac{\partial^-}{\partial \eta}\mathbf{B}^+ + \frac{\partial^+}{\partial \eta}\mathbf{B}^- + \frac{\partial'}{\partial \eta}\mathbf{B}_v\right\}\Delta\hat{\mathbf{q}} = \frac{\mathbf{V}}{\Delta t}\Delta\hat{\mathbf{q}}^* \quad (11)$$

where $\mathbf{A}$ and $\mathbf{B}$ refer to the approximate convective flux Jacobians and $\mathbf{A_v}$ and $\mathbf{B_v}$ are the viscous flux Jacobians. The cell volume and timestep are defined as $\mathbf{V}$ and Δt, respectively. The time integration is complete given that

$$\mathbf{RHS} = -\left\{\frac{\partial\left(\hat{\mathbf{f_1}}+\hat{\mathbf{g_1}}\right)}{\partial \xi} + \frac{\partial\left(\hat{\mathbf{f_2}}+\hat{\mathbf{g_2}}\right)}{\partial \eta}\right\} \quad (12)$$

and by defining the update $\mathbf{q}^{\hat{n+1}} = \mathbf{q}^{\hat{n}} + \Delta\hat{\mathbf{q}}$. The notation $(\partial^+, \partial^-, \partial')$ refers to the forward, backward, and central difference operators, respectively. The approximate convective flux Jacobian $\mathbf{A}^{\pm} = \mathbf{R}\Lambda^{\pm}\mathbf{L}$ is defined in terms of eigenvalues and the left and right eigenvectors, shown here for completeness.

$$\Lambda = \begin{bmatrix} U_c+a & 0 & 0 \\ 0 & U_c & 0 \\ 0 & 0 & U_c-a \end{bmatrix}, \ \Lambda^{\pm} = \frac{(\Lambda \pm |\Lambda|)}{2} \quad (13)$$

The contravariant velocity is defined in terms of the metrics which correspond to both generalized coordinate directions (ξ,η), depending on which Jacobian is being formed.

$$U_c = n_x \mathrm{U} + n_y \mathrm{V}$$
$$N = n_x^2 + n_y^2 \quad (14)$$
$$n \in (\xi, \eta)$$

The LHS was discretized to first order accuracy; however, the RHS was based upon the second order accurate upwind TVD scheme of Chakravarthy and Osher[17]. The approximate Riemann solver and variable extrapolation technique are described in Gorski[15]. The interested reader is encouraged to examine this reference for further details. It was not necessary to utilize the limiter function in order to get a smooth solution for the RANS equations.

Right Eigenvectors		
$-a(U_c-a)$	0	$-a(U_c+a)$
$-n_x(U_c-a)+\mathrm{U}N$	$-n_y$	$n_x(U_c+a)-\mathrm{U}N$
$-n_y(U_c-a)+\mathrm{V}N$	n_x	$n_y(U_c+a)-\mathrm{V}N$

Table 4 The right eigenvectors of the 2D incompressible RANS equations

Left Eigenvectors		
$\frac{1}{2a^2}$	$\frac{n_x(U_c+a)}{2a^2N}$	$\frac{n_y(U_c+a)}{2a^2N}$
$\frac{Un_y-Vn_x}{a^2}$	$-\frac{VU_c+n_y\beta}{a^2}$	$\frac{UU_c+n_x\beta}{a^2}$
$-\frac{1}{2a^2}$	$-\frac{n_x(U_c-a)}{2a^2N}$	$-\frac{n_y(U_c-a)}{2a^2N}$

Table 5 The left eigenvectors of the 2D incompressible RANS equations

Turbulent Transport Equations

The approximate factorization technique was also applied to the turbulent transport equations 3. For two dimensional flow, the system is expressed as follows:

$$\begin{aligned}
&\frac{\partial}{\partial t}(\mathbf{q}^t)+\frac{\partial}{\partial x}(\mathbf{f}_1^t+\mathbf{g}_1^t)+\frac{\partial}{\partial y}(\mathbf{f}_2^t+\mathbf{g}_2^t)=\mathbf{S}^t\\
&\mathbf{q}^t=\begin{bmatrix}k\\ \epsilon\end{bmatrix},\ \mathbf{f}_1^t=\begin{bmatrix}Uk\\ U\epsilon\end{bmatrix},\ \mathbf{f}_2^t=\begin{bmatrix}Vk\\ V\epsilon\end{bmatrix}\\
&\mathbf{g}_1^t=\frac{-1}{Re}\begin{bmatrix}\nu_k\frac{\partial k}{\partial x}\\ \nu_\epsilon\frac{\partial \epsilon}{\partial x}\end{bmatrix},\ \mathbf{g}_2^t=\frac{-1}{Re}\begin{bmatrix}\nu_k\frac{\partial k}{\partial y}\\ \nu_\epsilon\frac{\partial \epsilon}{\partial y}\end{bmatrix}\\
&\mathbf{S}^t=\frac{1}{Re}\begin{bmatrix}\mathcal{P}-\epsilon Re+\mathrm{D}\\ \mathrm{C_1f_1}\frac{\epsilon}{k}\mathcal{P}-\mathrm{C_2f_2}\frac{\epsilon^2}{k}Re+\mathrm{E}\end{bmatrix}
\end{aligned}\tag{15}$$

with $\nu_k=\nu+\frac{\nu_t}{\sigma_k}$, $\nu_\epsilon=\nu+\frac{\nu_t}{\sigma_\epsilon}$ and the production term $\mathcal{P}=\nu_t\left\{2\left[\left(\frac{\partial U}{\partial x}\right)^2+\left(\frac{\partial V}{\partial y}\right)^2\right]+\left(\frac{\partial U}{\partial y}+\frac{\partial V}{\partial x}\right)^2\right\}$. After transforming the equations into generalized coordinates, the system was approximately factored as:

$$\begin{aligned}
&\left\{\frac{\mathbf{V}}{\Delta t}+\frac{\partial^-}{\partial\xi}\mathbf{A}^{t+}+\frac{\partial^+}{\partial\xi}\mathbf{A}^{t-}+\frac{\partial'}{\partial\xi}\mathbf{A}_v^t-\alpha_\xi\mathbf{H}^t\right\}\Delta\hat{\mathbf{q}}^{t*}=\mathbf{RHS}^t\\
&\left\{\frac{\mathbf{V}}{\Delta t}+\frac{\partial^-}{\partial\eta}\mathbf{B}^{t+}+\frac{\partial^+}{\partial\eta}\mathbf{B}^{t-}+\frac{\partial'}{\partial\eta}\mathbf{B}_v^t-\alpha_\eta\mathbf{H}^t\right\}\Delta\hat{\mathbf{q}}^t=\frac{\mathbf{V}}{\Delta t}\Delta\hat{\mathbf{q}}^{t*}\\
&\mathbf{RHS}^t=-\frac{\partial\left(\hat{\mathbf{f}}_1^t+\hat{\mathbf{g}}_1^t\right)}{\partial\xi}-\frac{\partial\left(\hat{\mathbf{f}}_2^t+\hat{\mathbf{g}}_2^t\right)}{\partial\eta}+\mathbf{S}^t
\end{aligned}\tag{16}$$

Evaluation of the LR source terms for the CH model was straightforward. However, the other three LR models required an evaluation of the volume integrals:

$$\begin{aligned}
&\int\int_V(\mathrm{U_{i,jk}})^2\mathrm{d}v\equiv\overline{\overline{(\mathrm{U_{i,jk}})^2}}\mathbf{V}\\
&\int\int_V\left[\left(\sqrt{k}\right)_{,i}\right]^2\mathrm{d}v\equiv\overline{\overline{\left[\left(\sqrt{k}\right)_{,i}\right]^2}}\mathbf{V}
\end{aligned}\tag{17}$$

The following second order accurate linearizations were implemented:

$$\begin{aligned}
&\overline{\overline{(\mathrm{U_{i,jk}})^2}}=\left(\overline{\overline{\mathrm{U_{i,jk}}}}\right)^2+O(\Delta x^2,\Delta y^2)\\
&\overline{\overline{\left[\left(\sqrt{k}\right)_{,i}\right]^2}}=\left(\overline{\overline{\left[\left(\sqrt{k}\right)_{,i}\right]}}\right)^2+O(\Delta x^2,\Delta y^2)
\end{aligned}\tag{18}$$

The convective flux Jacobian for system 16 is equal to the identity matrix multiplied by the contravariant velocity, U_c. The eigenvalue matrix is equivalent to the convective flux Jacobian matrix. Thus the left and right eigenvector matrices are both equal to the identity matrix. This permits a straightforward application of the same techniques used upon the flow equations 11.

Michelassi and Shih[12] proposed a linearization for the source term Jacobian $\mathbf{H}^t$ based upon retaining the positive leading order terms. After considerable effort, a similar formulation was found to be the most effective. These terms are shown in table 6. All off diagonal terms were set to zero so as not to impede diagonal dominance. The coefficients (α_ξ,α_η) were used to include the implicit treatment of the source terms in both directions as needed for elliptic flows. The convergence was best when both were set equal to one half. The TVD variable extrapolation is used for resolving the right hand side of this system, also. The limiter function is necessary for this system to avoid the nonphysical overshoots introduced by the linearization of $\mathbf{H}^t$.

model	$\frac{\partial S_1^t}{\partial k}$	$\frac{\partial S_2^t}{\partial \epsilon}$
JL	$-\frac{\epsilon}{k}$	$-C_2f_2\frac{\epsilon}{k}$
LS	$-\frac{\epsilon}{k}$	$-C_2f_2\frac{\epsilon}{k}$
CH	$-\frac{2}{Re_ty^2}$	$\frac{E}{\epsilon}$
SL	$-\frac{\epsilon}{k}$	$-2C_2f_2\frac{\epsilon}{k}$
HR	0	0

Table 6 Diagonal terms for the approximate source Jacobian, $\mathbf{H}^t$

BFS Flow: Numerical Configuration

The numerical domain extended 15H upstream and 60H downstream of the step. These values were found to generate results independent of the inlet and exit locations, respectively. A mesh is constructed from three individual blocks with shared boundaries. However, the grid dimensions will be referred to as the total number of cells in each direction over the entire domain. Recently, Thangam and Hur[18] found that for a 1:3 tunnel configuration, a 166x73 cell Cartesian grid was necessary to fully resolve the flow features using a HR model. This grid was stretched towards the step in the streamwise (x) direction and uniform in the transverse (y) direction. However, due to the different nature of this 1:9 tunnel configuration, a separate grid independence study was carried out for the HR formulation.

Three grids were used in the mesh dependence study. Due to the assumptions of the wall function given in equation 4, the normal distance from the wall to the first cell center was specified to yield $y^+\approx 30$ for regions

outside the recirculation zones. The three grids examined were 62x40, 122x80, and 250x160 cells. Figure 2 demonstrates the grid independence of the medium sized mesh results using profiles of the velocity and turbulence quantities at five step heights downstream of the step. By examining just the velocity data, one might assume that grid independence is achieved using the coarsest grid. However, the turbulence profiles reveal an improvement between the coarse and medium mesh results. The differences between the medium and fine mesh predictions for all quantities are negligible. Thus, the medium grid of 122x80 cells was chosen to conduct the HR testing on. For the LR formulations, the near-wall grid spacing was dictated by a discretization criterion of $y_1^+ \approx 1.0$ for the first cell along a no-slip boundary. Furthermore, 15–20 cells were placed below the $y^+ \approx 30.0$ location. The LR grid was adapted using TurboI[19] so that the thin layer of high aspect ratio cells, necessary to resolve the separating shear layer, did not extend through the whole numerical domain. The mesh configurations used can be seen in figure 3 below.

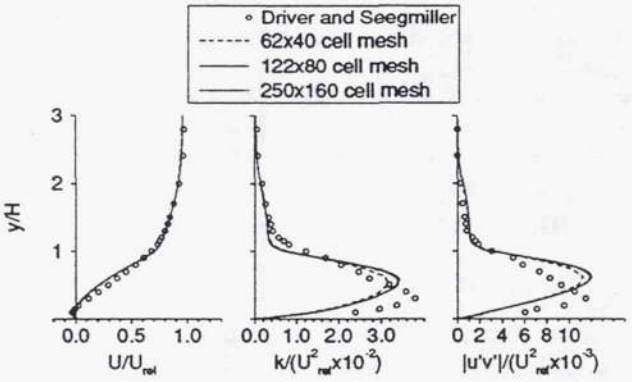

Fig. 2 Mesh refinement study: velocity and turbulence profiles downstream of the step at $x/\mathrm{H} = 5$.

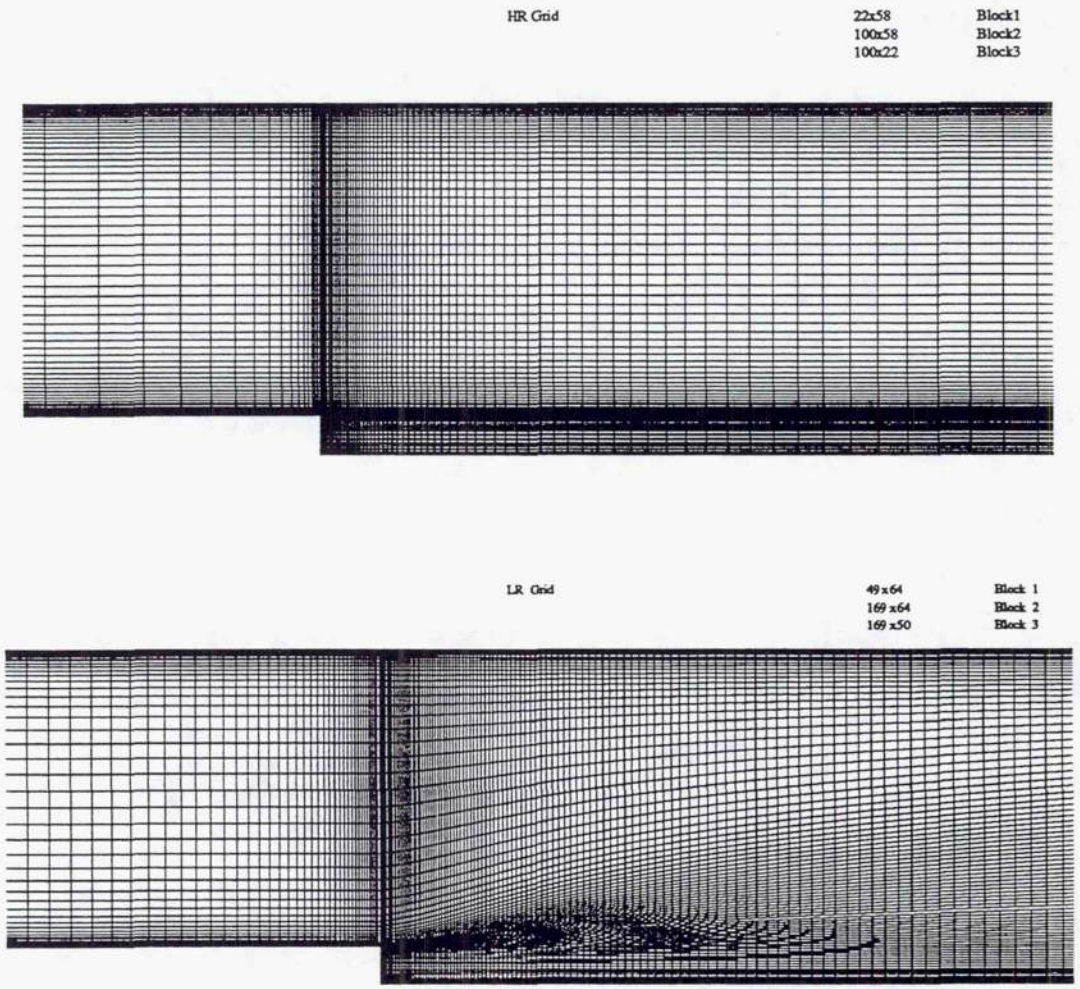

Fig. 3 Multiblock mesh configuration for the HR and LR k-ϵ models

Experimental data for the mean velocity and turbulent intensity profiles are available for the inlet tunnel at a location four step heights upstream of separation. These values were used at the numerical inlet. Pitot tube measurements of the velocity profiles helped to insure a reasonable massflow rate at the inlet. This was critical to proper resolution of the pressure drop across the tunnel. However, the boundary layer along the wall opposite the step was not accurately resolved using the laser Doppler velocimeter. Thus, the profiles of the turbulent quantities were mirrored about the inlet tunnel centerline. Even though the conditions were applied at fifteen step heights upstream of separation, the effect upon the result is negligible. Figure 4 demonstrates that the comparison between experiment and calculation at four step heights upstream from separation is good.

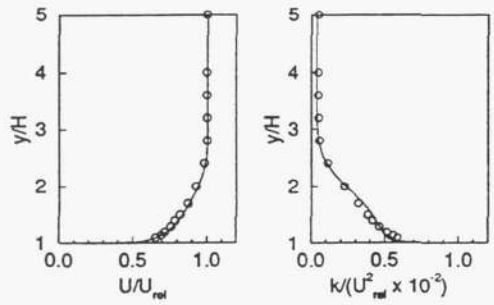

Fig. 4 Inlet tunnel conditions at x/H=-4.0

The velocities were specified and pressure was extrapolated at inlet, and vice versa at exit. For the turbulence equations, both k and ϵ were specified at inlet and extrapolated at exit. Using the two turbulent intensity profiles, a kinetic energy profile was estimated using $k = \frac{3}{4}(\overline{uu} + \overline{vv})$. This implied that the third component was an average of the other two. Kjelgaard's results[14] support this assumption. The value for the mixing length (l_m) was calculated using the simple ramp function[20] described in figure 5.

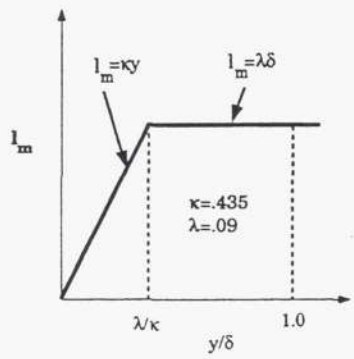

Fig. 5 Ramp function definition of turbulent length scale

Results

The primary reattachment length is often used for measuring the overall performance for backward-facing step flow calculations. The experimental reattachment length for this tunnel geometry was given by Driver and Seegmiller as 6.26H. Numerically, this value was extrapolated from the velocity field and corresponds to the location where the value of wall shear stress was zero. The results are shown here in table 7. The LS, CH and HR performed the best, followed by the SL and JL models.

model	JL	LS	CH	SL	HR
x_r	4.9	5.4	5.4	5.1	5.5

Table 7 Primary reattachment length

The velocity fields predicted by all five models were nearly identical. The superimposed profiles of figure 6 clearly indicate this. Except for the reattachment region, the velocity profiles were indistinguishable. They have been plotted merely to demonstrate this point. The wall static pressure coefficient, shown in figure 7 below, was more helpful in discriminating between the various model results. The trends evident in the reattachment length data were echoed here for the pressure rise along the stepside wall, with the exception of the Chien result. It should be noted that all five formulations underpredicted the pressure drop in the recirculating flow and overpredicted the pressure rise near reattachment. The CH model underpredicted the pressure rise more than any other technique, while the LS model yielded the best agreement with the experimental data. The HR model has an especially difficult problem in predicting the proper coefficient in the redeveloping flow region, although all four LR models overpredict this value to some degree as well. This might be a result of a slight error in massflow rate. This offset is also visible in the numerical results of Sindir[4].

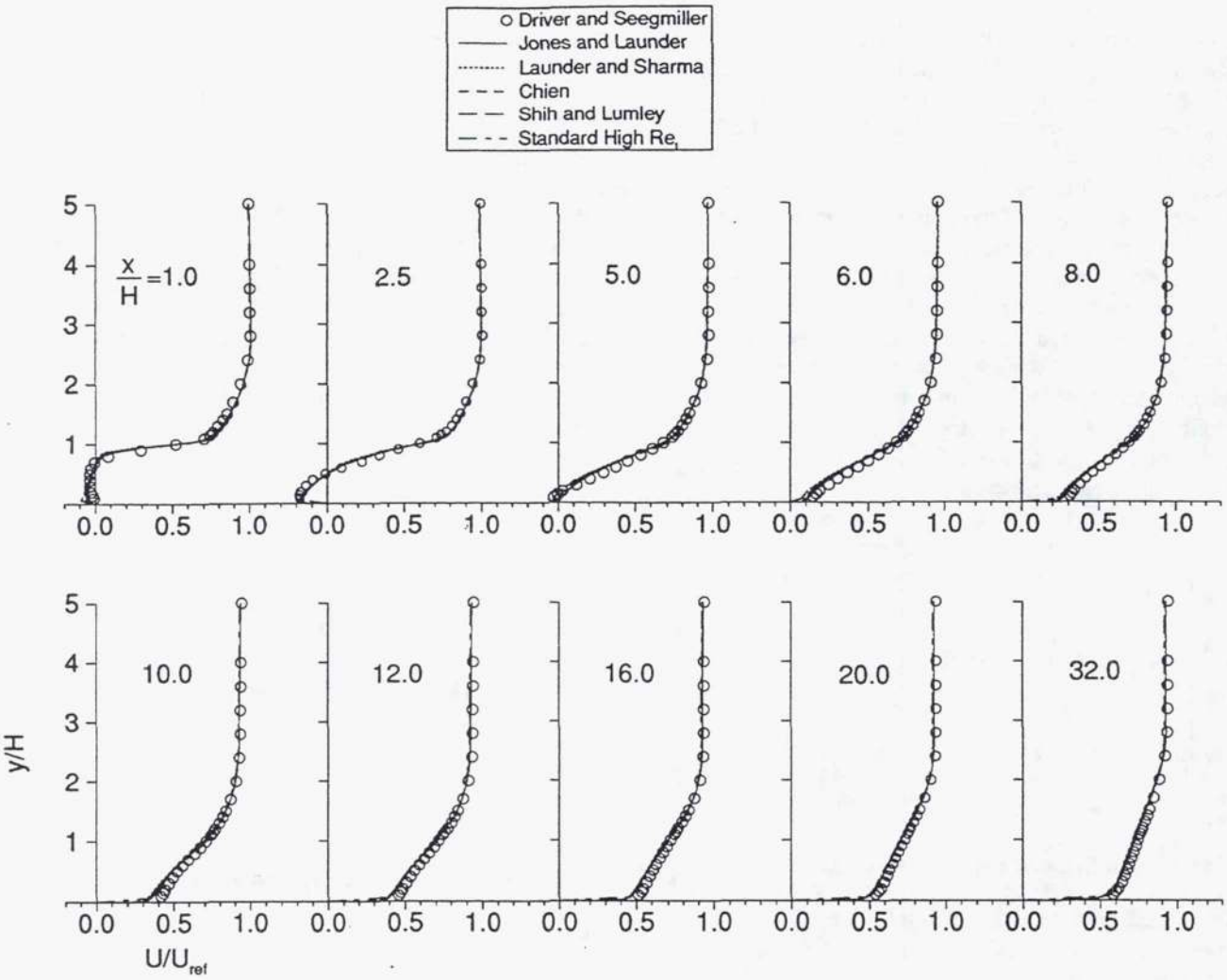

Fig. 6 Mean velocity profiles downstream of the step

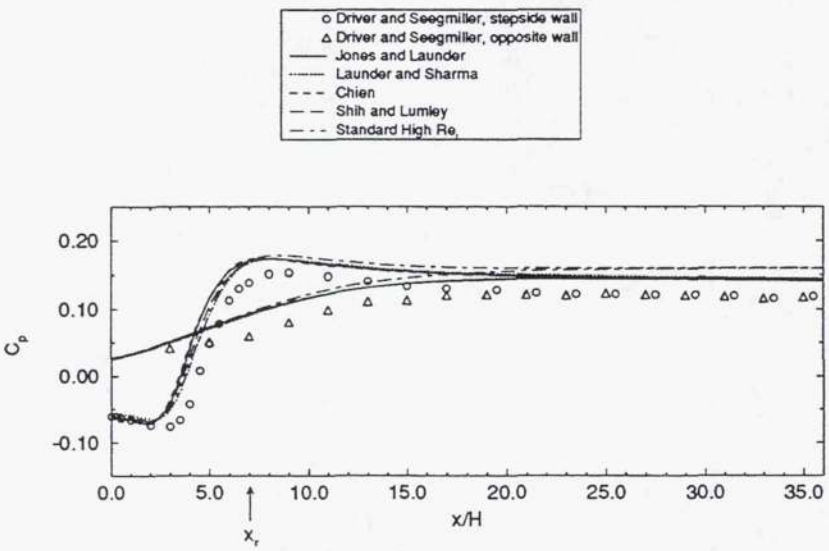

Fig. 7 Wall static pressure coefficient downstream of the step

The profiles for the turbulent kinetic energy are also shown below. In the neighborhood of reattachment, the peak values were consistently located too far from the wall. In figure 8 the profiles at $\frac{x}{H} = 1$ agree in location and magnitude for the peak value of k. Behavior within the recirculation bubble was best predicted here by the Chien model. The data at $\frac{x}{H} = 2.5$ appeared the most irregular and it is difficult to say which model performs best. The predictions appear to vary the most at this location. The turbulent kinetic energy was not well predicted by any technique for the next three profiles shown. However, the differences between the five k-ϵ models are becoming much smaller. The peak values were also slightly overestimated. The remaining five profiles, beginning with $\frac{x}{H} = 10$, describe the recovery of redeveloping channel flow. The models overestimated the turbulent kinetic energy of the reattached shear layer initially, but this was significantly improved after $\frac{x}{H} = 20$. For the HR model, the peak values of k are slightly lower throughout the redeveloping flow region. It should be noted that overall, the standard HR k-ϵ model predicts similar results to the LR formulations for the turbulent kinetic energy, except in the region of high gradient near the separation line. This can be most easily seen in the first four profiles near $y/H = 1.0$.

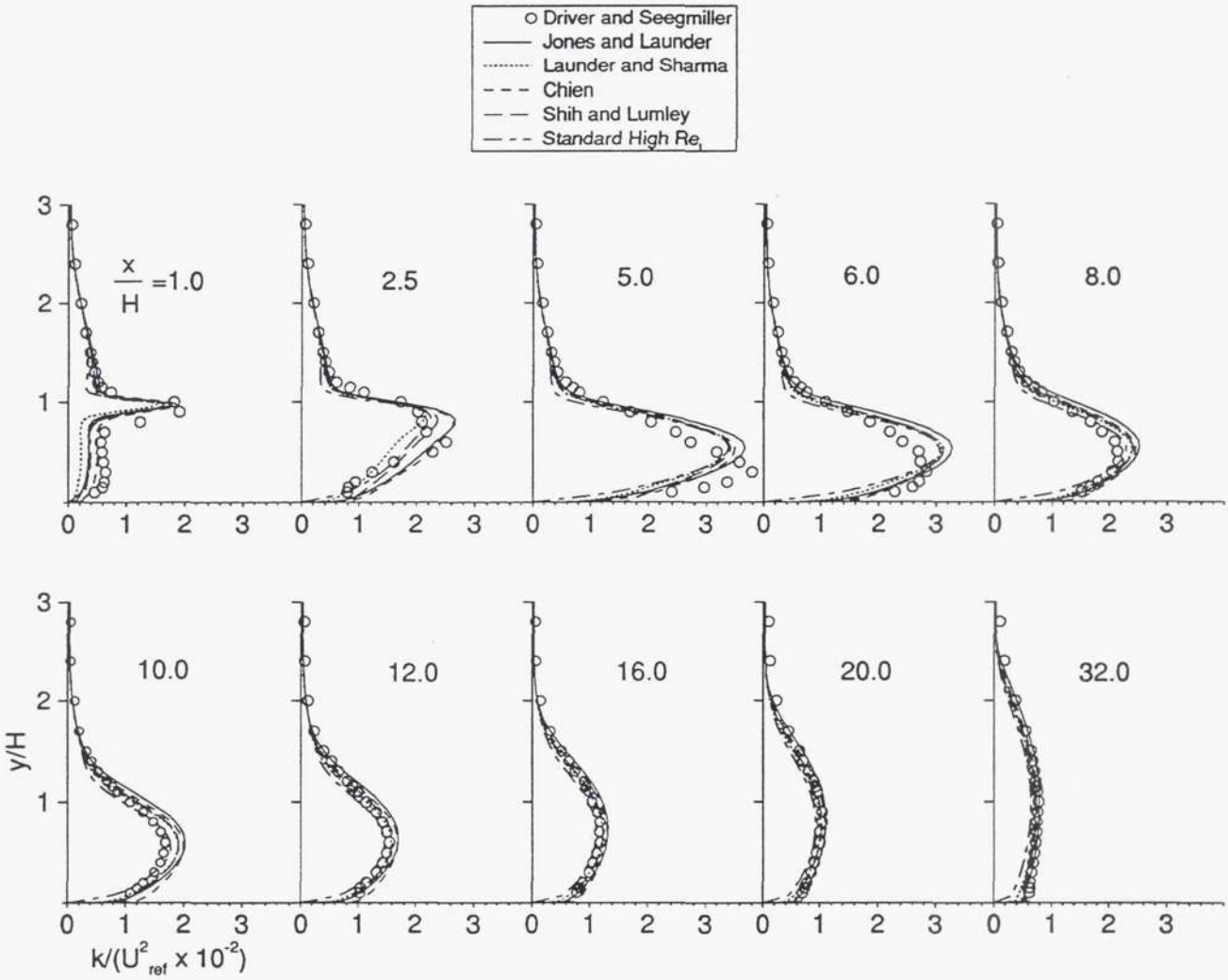

Fig. 8 Turbulent kinetic energy profiles downstream of the step

Similar behavior was observed in the prediction of the turbulent shear stress shown in figure 9. Relatively good agreement was exhibited for all models at the $\frac{x}{H} = 1$ location. However, by $\frac{x}{H} = 2.5$ the peak value of turbulent shear was overpredicted by the JL and CH models. Also, the vertical position was located too far from the wall. It is interesting to note that the various LR profiles are bracketed here by the maximum values of JL and the minimum of LS. These two differ only in the damping function f_μ and the constants C_1 and C_2. As one proceeded downstream towards reattachment, the differences between models were reduced and the overpredictions more pronounced. After reattachment, the various k-ϵ models continued to overpredict the turbulent shear stress even throughout the recovery zone, although this effect was reduced as the exit was approached. Note that the HR results were predicting peak values slightly lower than the LR models.

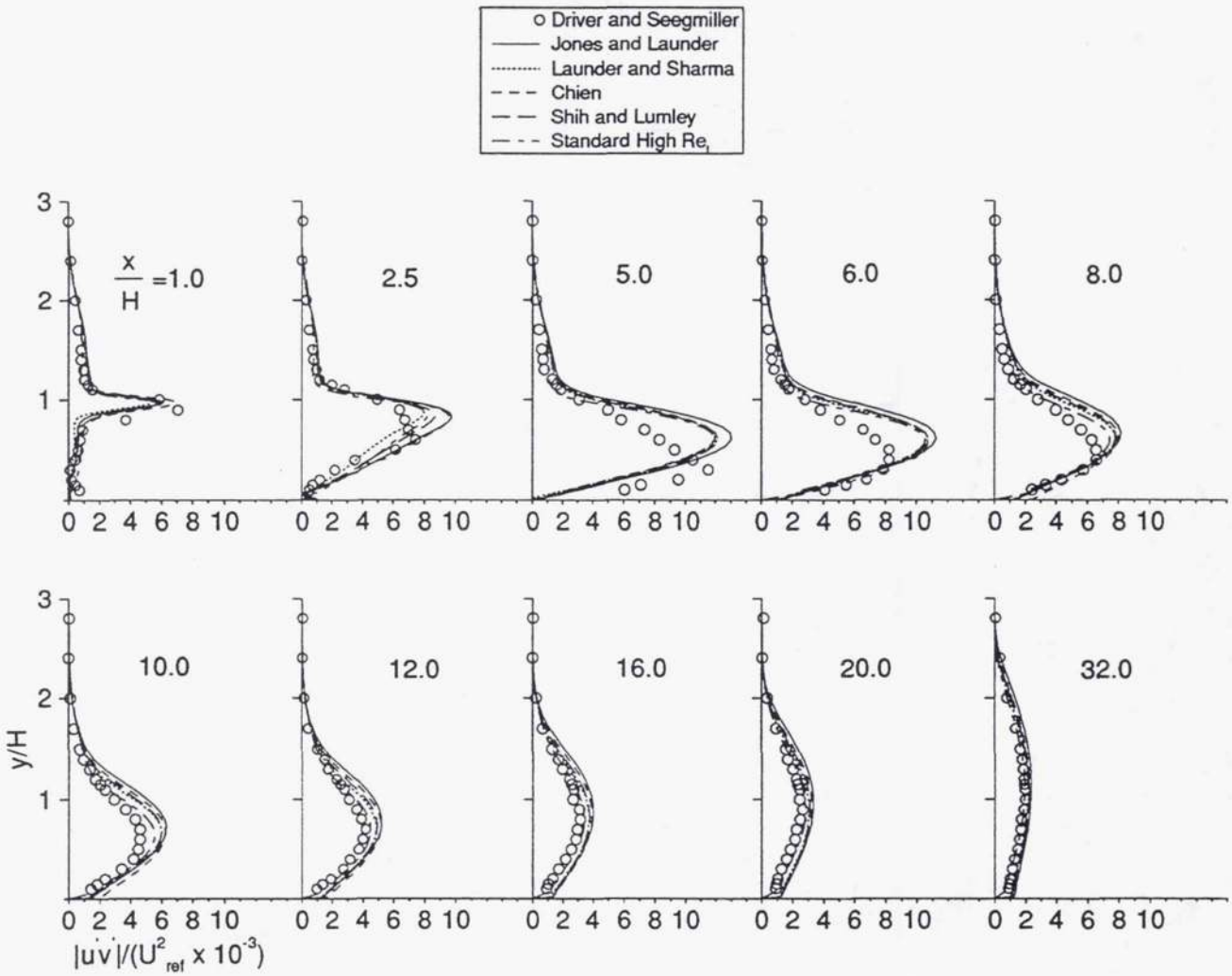

Fig. 9 Turbulent shear stress profiles downstream of the step

For the backward-facing step flow, prediction of the skin friction coefficient along the stepside wall was the most difficult task. Results for the five models tested are given below in figure 10. The HR formulation predicted the wall shear stress better than any of the LR formulations tested. However, all of the models have inaccurately predicted the near-wall velocity gradient for the recirculating flow close to reattachment. The Chien model yielded the largest overshoot in C_f. This was in contrast to the relatively good reattachment length prediction of table 7. However, an examination of the Chien damping function f_μ indicated a dependence upon the y^+ parameter, or the nearest wall shear stress. In the neighborhood of a separation or reattachment point, an anomalous region of very low eddy viscosity results due to excessive damping in the neighborhood of zero wall shear stress. Figure 11 below demonstrates the effect of this y^+ dependence on the calculation of eddy viscosity. The behavior of the SL model in figure 12 was typical of the JL, LS, and HR results.

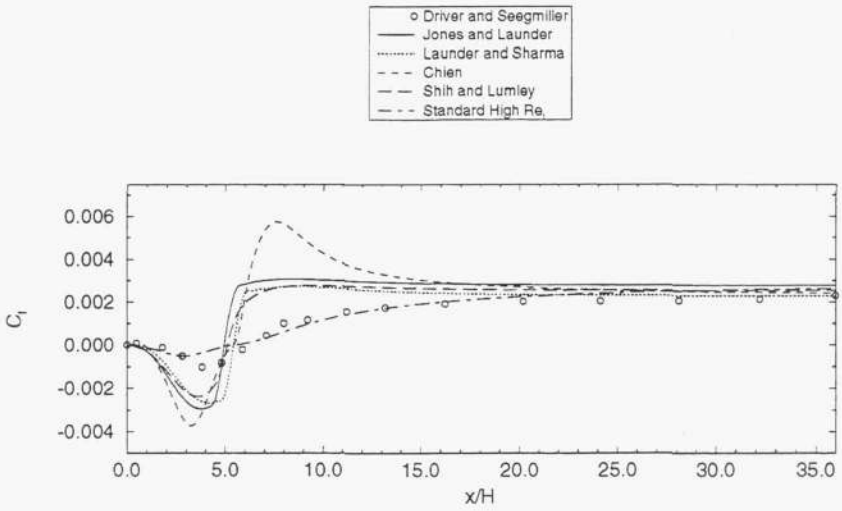

Fig. 10 Friction coefficient for the stepside wall downstream of the step

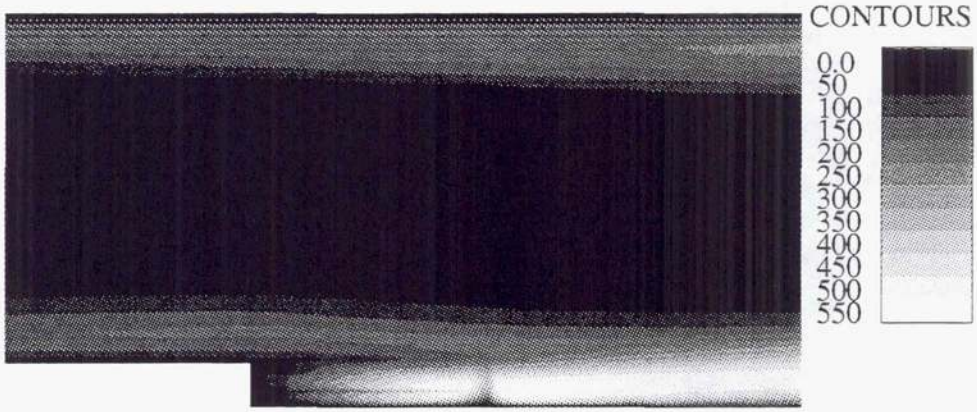

Fig. 11 Nondimensional eddy viscosity field for the CH model

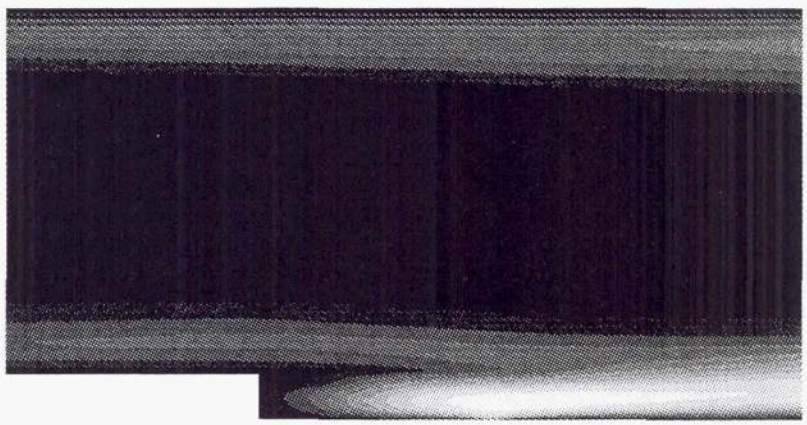

Fig. 12 Nondimensional eddy viscosity field for the SL model

Close examination of the experimental skin friction data indicates a small corner eddy was present at $\frac{x}{H} = 0.5$. However, by $\frac{x}{H} = 1.8$ the primary recirculation zone was encountered. Numerical evidence of the corner eddy was demonstrated by two of the LR models: CH and SL. The JL, LS and HR formulations did not reveal any secondary recirculation zones. See table 8 below. This zone was confined to a very small region in the corner where the Re_t values are low.

A trend in the length of this secondary recirculation zone can be correlated to the damping function used in the definition of eddy viscosity for the LR models. Following the example of Patel et al.[11], the damping functions were examined for attached boundary layer flows. From figure 13 we can see that for the JL and LS models, the damping in the viscous sublayer was never complete because the functions tend to small positive values instead of zero. In addition, there is a steep rise in the damping function around $y^+ \approx 10$. The SL and CH models both damped the eddy viscosity to zero at the wall, and also diffused the viscous effects further out from the wall. The most diffusive of the near-wall treatments was indeed the CH model. The largest secondary recirculation bubble also corresponds to the CH calculation. It appears that the interplay between the near-wall, viscous dominated flow and the fully turbulent, high Re_t flow is critical to proper resolution of this corner region. However, more experimental and numerical work needs to be undertaken before any meaningful conclusions can be drawn.

model	JL	LS	CH	SL
x_{r2}	0.0	0.0	0.8	0.1

Table 8 Secondary flow reattachment length

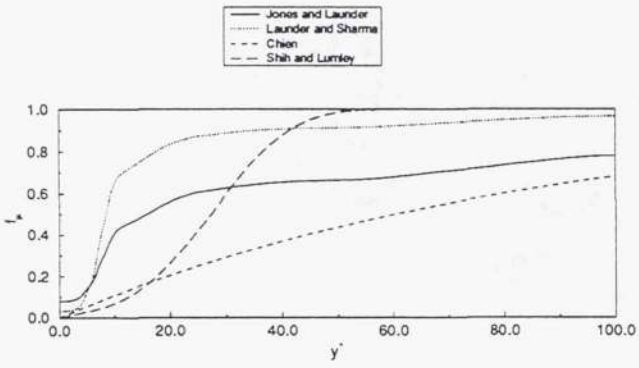

Fig. 13 Damping function behavior for attached boundary layer flow

The preceding calculations were carried out on the Cray YMP at NASA Lewis. On average, a LR calculation needed roughly 5000 iterations to converge (CFL=3.0), depending upon the quality of the initial condition. Likewise, a HR calculation required approximately 3300 iterations to converge to the same extent. The convergence criterion was based upon the L_2 norm of the transient terms dropping five orders in magnitude. This was realized in all but the LS model, which tended to level off after a drop of three and a half orders.

Conclusion

Results for flow over the backward-facing step tunnel configuration of Driver and Seegmiller were calculated for the standard HR, and four LR k-ϵ models. The velocity profiles and pressure coefficient data demonstrated how similar the results were among all five formulations. Slight differences appeared in the vicinity of reattachment. All five models underpredicted the redeveloping flow velocity profiles. Similarly, all five models yielded an early prediction of the pressure rise. A more discriminating measure of the near-wall velocity field was the reattachment length, x_r. This was tabulated in table 7. It appeared that the LS, CH, and HR models yielded similar performances in underpredicting this parameter by approximately 14%. Examination of the experimental velocity data near reattachment indicates that the reversed flow is confined to a very thin near-wall region; perhaps an improved damping strategy can be devised to resolve this low Re_t region. However, I believe that the accurate prediction of skin friction is the most significant challenge to the LR k-ϵ models for backward-facing step flow.

Only the HR technique can claim to predict the wall shear stress in a bounded sense. The SL model produced the best prediction of the LR techniques, while the CH model produced the least reliable wall shear stress prediction. This appeared to be a result of the y^+ based damping function, f_μ. I believe that a modification to the CH damping function which reduces this local separation/reattachment effect may improve the shear stress prediction.

The turbulent kinetic energy and shear stress profiles were generally overpredicted in the recirculation zone. The position of the peak values were consistently located too far from the wall as well. Perhaps the strong anisotropy of the flow contributes to this. Two anisotropic eddy viscosity models[5,21] have been reported to improve behavior for this flow.

The significant conclusion of this study is that the assumption of local equilibrium inherent in the wall function technique yields a credible result for separated flow. This conclusion is shared by So et al.[2] Furthermore, the near-wall modelling techniques employed in the JL, LS, SL, and CH appear to be much more sensitive to adverse pressure gradients than does the HR formulation. It is apparent that LR models do not adequately resolve the near-wall velocity gradient. However, different LR for-

mulations yield significantly different near-wall predictions as evidenced by the skin friction results. Of the four LR models examined, the SL technique yields the most accurate prediction for the backward-facing step flow in the 1:9 channel geometry. However, the standard HR k-ϵ model is still superior due to the more accurate prediction of the skin friction behavior along the step side wall.

Acknowledgments

The author would like to thank Lisa Beard of the University of Michigan, and Tsan-Hsing Shih of CMOTT for their respective contributions to this work.

References

[1] Purtell, L. P., "Turbulence in Complex Flows: A Selected Review," AIAA paper 92-0435, 1992.

[2] So, R. M. C., Lai, Y. G., Hwang, B. C., and Yoo, G. J., "Low-Reynolds-number modelling of flows over a backward-facing step," *Journal of Applied Mathematics and Physics (ZAMP)*, Vol. 39, 1988, pp. 13–27.

[3] Avva, R. K., Smith, C. E., and Singhal, A. K., "Comparitive study of high and low Reynolds number versions of k-ϵ models," AIAA paper 90-0246, 1990.

[4] Driver, D. M. and Seegmiller, H. L., "Features of a Reattaching Turbulent Shear Layer in Divergent Channel Flow," *AIAA Journal*, Vol. 23, no. 2, 1985, pp. 163–171.

[5] Thangam, S. and Speziale, C. G., "Turbulent Separated Flow Past a Backward Facing Step: a Critical Evaluation of Two-Equation Turbulence Models," *AIAA Journal*, Vol. 30, no. 5, 1992, pp. 1314–1320.

[6] Jones, W. P. and Launder, B. E., "The Prediction of Laminarization with a Two-Equation Model of Turbulence," *International Journal of Heat and Mass Transfer*, Vol. 15, 1972, pp. 301–314.

[7] Chien, K.-Y., "Predictions of Channel and Boundary-Layer Flows with a Low-Reynolds-Number Turbulence Model," *AIAA Journal*, Vol. 20, no. 1, 1982, pp. 33–38.

[8] Launder, B. E. and Sharma, B. I., "Application of the Energy-Dissipation Model of Turbulence to the Calculation of Flow near a Spinning Disc," *Letters in Heat and Mass Transfer*, Vol. 1, 1974, pp. 131–138.

[9] Shih, T.-H. and Lumley, J. L., "Kolmogorov Behavior of Near-Wall Turbulence and Its Application in Turbulence Modeling," NASA Technical Memorandum 105663, 1992.

[10] Lang, N. J. and Shih, T.-H., "A Critical Comparison of Two-Equation Turbulence Models," NASA Technical Memorandum 105237, 1991.

[11] Patel, V. C., Rodi, W., and Scheuerer, G., "Turbulence Models for Near-Wall and Low Reynolds Number Flows: A Review," *AIAA Journal*, Vol. 23, no. 9, 1985, pp. 1308–1319.

[12] Michelassi, V. and Shih, T.-H., "Elliptic Flow Computation by Low Reynolds Number Two Equation Turbulence Models," NASA Technical Memorandum 105376, 1991.

[13] Kim, J., Kline, S. J., and Johnston, J. P., "Investigation of Separation and Reattachment of a Turbulent Shear Layer. Flow over a Backward-Facing Step.," Stanford University Technical Report MD-37, 1978.

[14] Kjelgaard, S. O., "Three Component Laser Velocimeter Surveys of the Flow over a Backward-Facing Step," *Laser Anemometry: Advances and Applications*, Vol. 2, edited by A. Dybbs and B. Ghorashi, 1991, pp. 529–539.

[15] Gorski, J. J., "TVD Solutions of the Incompressible Navier-Stokes Equations With an Implicit Multigrid Scheme," *Proceedings of the AIAA/ASME/SIAM/APS 1st National Fluid Dynamics Congress*, Vol. 1, 1988, pp. 394–401.

[16] Chorin, A. J., "A Numerical Method for Solving Incompressible Viscous Flow Problems," *Journal Computational Physics*, Vol. 2, 1967, pp. 12–26.

[17] Chakravarthy, S. R. and Osher, S., "A New Class of High Accuracy TVD Schemes for Hyperbolic Conservation Laws," AIAA paper 85-0363, 1985.

[18] Thangam, S. and Hur, N., "A Highly Resolved Numerical Study of Turbulent Separated Flow Past a Backward-Facing Step," *International Journal of Engineering Science*, Vol. 29, no. 5, 1991, pp. 607–615.

[19] Choo, Y. K., Miller, D. P., and Reno, C. J., "Implementation of Control Point Form of Algebraic Grid-Generation Technique," NASA Technical Memorandum 103748, 1991.

[20] Rodi, W., *Turbulence Models and their Application in Hydraulics: A State of the Art Review*, International Association for Hydraulics Research, 1980.

[21] Shih, T.-H., Zhu, J., and Lumley, J. L., "A Realizable Reynolds Stress Algebraic Equation Model," NASA Technical Memorandum 105993, Cleveland, Ohio, 1992.

REPORT DOCUMENTATION PAGE

Form Approved
OMB No. 0704-0188

1. AGENCY USE ONLY (*Leave blank*)	2. REPORT DATE	3. REPORT TYPE AND DATES COVERED
	June 1993	Technical Memorandum

4. TITLE AND SUBTITLE

A Critical Comparison of Several Low Reynolds Number k-ε Turbulence Models for Flow Over a Backward-Facing Step

5. FUNDING NUMBERS

WU–505–90–5K

6. AUTHOR(S)

C.J. Steffen, Jr.

7. PERFORMING ORGANIZATION NAME(S) AND ADDRESS(ES)

National Aeronautics and Space Administration
Lewis Research Center
Cleveland, Ohio 44135–3191

8. PERFORMING ORGANIZATION REPORT NUMBER

E–7873

9. SPONSORING/MONITORING AGENCY NAME(S) AND ADDRESS(ES)

National Aeronautics and Space Administration
Washington, D.C. 20546–0001

10. SPONSORING/MONITORING AGENCY REPORT NUMBER

NASA TM–106173
AIAA–93–1927
CMOTT–93–9

11. SUPPLEMENTARY NOTES

Prepared for the 29th AIAA Joint Propulsion Conference and Exhibit cosponsored by the AIAA, SAE, ASME, and ASEE, Monterey, California, June 28–30, 1993. C.J. Steffen, Jr., Center for Modeling of Turbulence and Transition, NASA Lewis Research Center, (work funded under NASA Cooperative Agreement NCC3-233). ICOMP Program Director, Louis A. Povinelli, (216) 433–5818.

12a. DISTRIBUTION/AVAILABILITY STATEMENT

Unclassified - Unlimited
Subject Category 64

12b. DISTRIBUTION CODE

13. ABSTRACT ***(Maximum 200 words)***

Turbulent backward-facing step flow was examined using four low turbulent Reynolds number k-ε models and one standard high Reynolds number technique. A tunnel configuration of 1:9 (step height: exit tunnel height) was used. The models tested include: the original Jones and Launder; Chien; Launder and Sharma; and the recent Shih and Lumley formulation. The experimental reference of Driver and Seegmiller was used to make detailed comparisons between reattachment length, velocity, pressure, turbulent kinetic energy, Reynolds shear stress, and skin friction predictions. The results indicated that the use of a wall function for the standard k-ε technique did not reduce the calculation accuracy for this separated flow when compared to the low turbulent Reynolds number techniques.

14. SUBJECT TERMS

Computational fluid dynamics; Turbulence models; Backward-facing step flow

15. NUMBER OF PAGES

16

16. PRICE CODE

A03

17. SECURITY CLASSIFICATION OF REPORT	18. SECURITY CLASSIFICATION OF THIS PAGE	19. SECURITY CLASSIFICATION OF ABSTRACT	20. LIMITATION OF ABSTRACT
Unclassified	Unclassified	Unclassified	